Cation-Induced Stabilization of the Engineered Cation-Binding Loop in Cytochrome *c* Peroxidase (CcP)†

B. Bhaskar,‡ Christopher A. Bonagura,‡,§ Huiying Li, and Thomas L. Poulos*

Departments of Molecular Biology and Biochemistry, Physiology and Biophysics and Program in Macromolecular Structure, University of California—Irvine, Irvine, California 92697-3900

Received August 1, 2001; Revised Manuscript Received December 4, 2001

ABSTRACT: We have previously shown that the K^+ site found in the proximal heme pocket of ascorbate peroxidase (APX) could be successfully engineered into the closely homologous cytochrome *c* peroxidase (CcP) [Bonagura et al., (1996) *Biochemistry 35*, 6107−6115; Bonagura et al. (1999) *Biochemistry 38*, 5538−5545]. In addition, specificity could be switched to binding Ca^{2+} as found in other peroxidases [Bonagura et al. (1999) *J. Biol. Chem. 274*, 37827−37833]. The introduction of a proximal cation-binding site also promotes conversion of the Trp191 containing cation-binding loop from a "*closed*" to an "*open*" conformer. In the present study we have changed a crucial hinge residue of the cation-binding loop, Asn195, to Pro which stabilizes the loop, albeit, only in the presence of bound K^+. The crystal structure of this mutant, N195PK2, has been refined to 1.9 Å. As predicted, introduction of this crucial hinge residue stabilizes the cation-binding loop in the presence of the bound K^+. As in earlier work, the characteristic EPR signal of Trp191 cation radical becomes progressively weaker with increasing [K^+] and the lifetime of the Trp191 radical also has been considerably shortened in this mutant. This mutant CcP exhibits reduced enzyme activity, which could be titrated to lower levels with increasing [K^+] when horse heart cytochrome *c* is the substrate. However, with yeast cytochrome *c* as the substrate, the mutant was as active as wild-type at low ionic strength, but ∼40-fold lower at high ionic strength. We attribute this difference to a change in the rate-limiting step as a function of ionic strength when yeast cytochrome *c* is the substrate.

Yeast cytochrome *c* peroxidase (CcP),[1] a biological redox partner of ferrocytochrome *c* (cyt *c*) for which high-resolution crystal structures are available (*1*, *2*) catalyzes the two-electron reduction of peroxide to water in a multistep reaction cycle as follows:

$$\underset{\text{Resting State}}{Fe^{3+}\ Trp} + H_2O_2 \rightarrow \underset{\text{Compound I}}{Fe^{4+}\text{-O Trp}^{\bullet}} + H_2O$$

$$\underset{\text{Compound I}}{Fe^{4+}\text{-O Trp}^{\bullet}} + \text{cyt. } c\ (Fe^{2+}) \rightarrow \underset{\text{Compound II}}{Fe^{4+}\text{-O Trp}} + \text{cyt. } c\ (Fe^{3+})$$

$$\underset{\text{Compound II}}{Fe^{4+}\text{-O Trp}} + \text{cyt. } c\ (Fe^{2+}) \rightarrow \underset{\text{Resting State}}{Fe^{3+}\ Trp} + \text{cyt. } c\ (Fe^{3+}) + H_2O$$

CcP first reacts with peroxide to give a stable intermediate where the two oxidizing equivalents of peroxide are stored on the iron as Fe^{4+}—O and as an amino acid free radical located on Trp191 (*3*−*6*). This oxidized state designated compound I, has a half-life of several hours in the absence of reductant (*7*). Compound I then is reduced by cyt *c* (Fe^{2+}) back to the resting state in two successive one-electron-transfer reactions. When yeast cyt *c* is the substrate, it appears that dissociation of cyt *c* from CcP at low ionic strength is limiting under steady-state conditions (*8*). At higher ionic strength electron-transfer processes become limiting (*8*). One remarkable aspect of this electron-transfer reaction is that the heme edges of the redox partners remain separated by no less than 18 Å, as revealed by the crystal structure of the noncovalent complex (*9*).

CcP consists of a 294-residue polypeptide with a single heme prosthetic group coordinated to His175. A unique feature of the CcP reaction cycle is the formation of a stable Trp cationic radical in compound I (*4*). Trp191 lies parallel to and in contact with proximal heme ligand, His175, situated just beneath the heme. Trp191 also is essential for CcP activity and critical for long-distance electron-transfer reaction from cyt *c* to CcP (*10*−*13*). Thus, the Trp191 radical constitutes an electron gate that allows the controlled

† This work was supported by grants from National Institutes of Health (Grant GM42615) and National Science Foundation. Portions of this research were carried out at the Stanford Synchrotron Radiation Laboratory, a national user facility operated by Stanford University on behalf of the U.S. Department of Energy, Office of Basic Energy Sciences. The SSRL Structural Molecular Biology Program is supported by the Department of Energy, Office of Biological and Environmental Research, and by the National Institutes of Health, National Center for Research Resources, Biomedical Technology Program, and the National Institute of General Medical Sciences.

* To whom the correspondence should be addressed at the Department of Molecular Biology and Biochemistry. Phone: (949) 824-7020. Fax: (949) 824-3280. E-mail: poulos@uci.edu.

‡ Equal contributions.

§ Current address: Plexxikon, Inc. 91 Bolivar Drive, Berkeley, CA 94710.

[1] Abbreviations: CcP, cytochrome *c* peroxidase; CcPK2, potassium-binding CcP; APX, ascorbate peroxidase; EPR, electron paramagnetic resonance; cyt *c*, reduced horse heart or yeast cytochrome *c*; EDTA, ethylenediaminetetraacetic acid; MPD, 2-methyl-2,4-pentanediol; DMI, 1,2-dimethylimidazolium; KPB, potassium phosphate buffer; MES, 4-morpholineethanesulfonic acid.

10.1021/bi011599y CCC: $22.00
Published on Web 02/01/2002

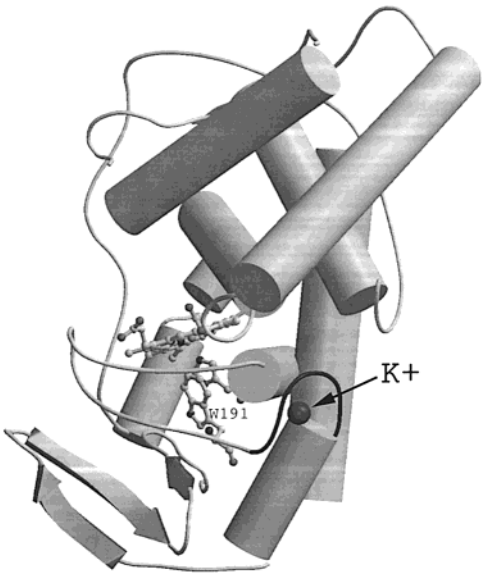

FIGURE 1: Schematic model of the CcP showing the location of engineered cation site. The darkened loop represents residues 192−199, which constitute the cation-binding loop. Trp191 is ~8 Å away from the cation.

reduction of peroxide, a two-electron oxidant, by cyt *c*, a one-electron reductant. Although the details of how electrons are transferred from reduced cyt *c* to CcP are unclear, the crystal structure of CcP-cyt *c* complex does indicate that cyt *c* binds near the 190−195 loop region of CcP (*9*). The CcP-cyt *c* co-crystal structure (*9*) together with a wealth of biochemical data indicates that each electron delivered from ferrocyt *c* is accepted by the Trp191 cationic radical (*14*, *15*) which explains why Trp191 is essential for activity (*16*).

Various experimental approaches (*15*−*18*) as well as theoretical calculations (*10*, *17*, *19*) support the view that the Trp191 radical is cationic, although there is not complete agreement on this point (*20*). Replacement of Trp191 by Gly leaves a cavity that binds a K^+ ion (*17*) as well as protonated forms of imidazole derivatives (*18*, *21*). In addition, computational methods (*10*, *17*, *19*) indicate that the electrostatic environment of the protein surrounding Trp191 is designed to stabilize the charge on the Trp191 cationic radical. A related heme peroxidase, ascorbate peroxidase (APX), contains a homologous Trp (Trp179) in the same position. Trp179 in APX sits directly adjacent to the proximal His163 ligand and donates a hydrogen bond to a conserved Asp residue exactly as in CcP. However, APX does not form a stable Trp-centered radical but, instead, a porphyrin π-cation radical (*22*), as in other peroxidases. This difference was attributed in part to the presence of K^+ ion bound within ~8 Å distance of the Trp179 of APX, which is absent in CcP (Figure 1). The proximal cation-binding loop (containing K^+ or Ca^{2+}) is characteristic of all peroxidases whose structures are known, except native CcP, where a water molecule occupies that position (Figure 1). The positively charged cation in APX helps to prevent formation of a stable Trp179 cationic radical owing to electrostatic destabilization (*10*, *22*, *23*). This hypothesis was tested by engineering the K^+ binding site of APX into CcP. The resulting CcP mutant, designated CcPK2, binds K^+ with high affinity and specificity, has only 1% of wild-type activity in the presence of K^+, and exhibits a significantly weakened EPR signal associated with the compound I Trp191 cationic radical (*10*, *24*). In addition to steady-state enzyme activity, single turnover electron transfer and the Trp191 EPR signal could be titrated with K^+. This indicated that binding of K^+ to the engineered site is responsible for loss in enzyme activity caused by the electrostatic destabilization of Trp191-containing cation-binding loop. However, the mutations required to introduce the cation-binding site into CcP also destabilized the cation-binding loop such that the loop more easily undergoes a large conformational change to an *open* conformation, where Trp191 moves ~10 Å toward the molecular surface as shown in cavity complementation experiments (*21*, *25*). To separate the effects of cation-binding and loop-stability, we have mutated a crucial hinge residue in CcPK2 of the cation-binding loop, Asn195, to the corresponding residue in APX, Pro. We find that the loop now favors a *closed* conformer, albeit, in the presence of K^+. Our goal was to distinguish in greater detail, the effects of electrostatic destabilization of Trp191 cationic radical and the structural/kinetic effects involved in cyt *c* binding to CcP at this surface loop. Here we present a detailed structural and functional analysis of this K^+ mutant, N195PK2.

MATERIALS AND METHODS

Materials. Enzymes and reagents for site-directed mutagenesis were purchased from Roche Molecular Biochemicals and New England Biolabs Inc. (Beverly, MA). Chromatography columns, media and Na^+/K^+ free Tris base were purchased from Amersham-Pharmacia Biotech. 1,2-Dimethylimidazolium (DMI), 2-methyl-2,4-pentanediol (MPD) and ion free phosphoric acid were purchased from Aldrich Chemicals. Horse heart and yeast cyt *c* and guaiacol were purchased from Sigma. All other chemicals were molecular biology grade or better and were purchased from Sigma or Fisher.

Site-Directed Mutagenesis. The cation-binding mutants of CcP were designated CcPK2 and N195PK2. CcPK2 has five amino acid substitutions corresponding to the cation-binding loop in APX. CcPK2 is altered at the following residue positions: A176T, G192T, A194N, T199D, and E201S as previously reported (*10*, *24*). N195PK2 has the substitution N195P on CcPK2 protein. Oligonucleotide-directed mutagenesis experiments were performed according to the method of Kunkel et al. (*26*) as described earlier (*10*, *24*) on pT7-7 vector that contained the CcPK2 gene (*10*) using an appropriate primer to get the desired mutation. All mutations were confirmed by DNA sequencing. To change the proximal Asn195 to Pro the following oligonucleotide was purchased from Operon Technologies, Inc. (Alameda, CA):

GGG CCA TGG **ACT** GCC AAT **CCC** AAC GTC TTT

The Asn195 on the CcPK2 template was replaced by Pro, the corresponding residue in APX and other peroxidases. Site-directed mutagenesis was carried out by annealing this oligomer to the single stranded uracylated CcPK2 template that was produced in *Escherichia coli* RZ1032 cells following the method of Kunkel et al. (*26*) as described previously (*27*, *28*). The mutagenic phosphorylated oligomer was boiled with template at a ratio of 20 pM oligomer to 1 pM template for 10 min and annealed for 15 min each at 70 °C, 37 °C, and then at room temperature, and finally on ice. Next, 1 mM

ATP was added with T4 DNA polymerase and T4 DNA ligase in excess to the reaction mixture and incubated at room temperature for 3−4 h followed by 4 °C overnight. The reaction mixture was then transformed by electroporation into competent MV1190 cells and colonies were selected under ampicillin resistance. Transformation efficiency was generally low, but transformants were likely to be positive clones without spontaneous mutations. Automated DNA sequencing was done at the UCI DNA sequencing core facility to ensure that introduced mutation was installed. The resultant protein variant was called N195PK2.

Protein Expression and Purification. Both wild-type CcP (WTCcP) and mutant CcP (CcPK2 and N195PK2) proteins were expressed under the control of T7 promoter in *E. coli* BL21(DE3) cells induced at A_{600} of 1.2−1.5 with 750 μM IPTG. Proteins were purified as previously described by Fishel et al. (*29*) and Choudhury et al. (*28*) with the exception of an FPLC anion exchange step introduced for CcPK2 using similar gradient parameters. After gel filtration on a Sephadex G-75 column and heme incorporation step by standard pH shift, CcPK2 was loaded on a 5 mL HiTrap-Q anion exchange column in 50 mM potassium phosphate buffer (KPB), pH 6.0, using an Amersham-Pharmacia Biotech FPLC. Stepping the gradient first to 80 mM, then to 130 mM KPB, and finally a linear gradient from 130 to 500 mM KPB, pH 6.0, eluted the protein. After heme incorporation and anion exchange chromatography, CcPK2 was crystallized by dialyzing against Milli-Q water. N195PK2 was produced in *E. coli* as a holo-protein and hence did not need heme incorporation step. N195PK2 was purified by a combination of gel filtration on Sephadex G-75 and DEAE-Sephacel anion exchange chromatography. Both WTCcP and mutant CcP proteins were stored as crystals at −80 °C in water. Mutant CcP concentrations were estimated spectrophotometrically using an extinction coefficient at 408 nm (ϵ_{408}) of 96 000 M^{-1} cm^{-1}.

Steady-State Activity Assays. The steady-state oxidation of horse heart and yeast cyt *c* (ferrocytochrome *c*) was measured at room temperature in a Cary 3E UV−visible spectrophotometer using a $\Delta\epsilon_{550}$ of 19 600 M^{-1} cm^{-1}. The initial linear change in optical density was used to calculate activities. Typical final reactions consisted of 25−30 μM dithionite-reduced horse heart or yeast cytochrome *c*, 180 μM H_2O_2, and 10 nM N195PK2 or 250 pM WTCcP in 5 mM or 100 mM Tris-phosphate, pH 6.0 (*30*). Hydrogen peroxide concentrations were standardized with $KMnO_4$ using the method of Fowler and Bright (*31*).

The ability of N195PK2 to oxidize small molecule substrates was determined using guaiacol and potassium ferrocyanide as substrates. The guaiacol peroxidase activity was determined in 50 mM Tris-phosphate, pH 6.0, containing 100 mM guaiacol, 600 μM H_2O_2, and 10 nM WTCcP or N195PK2 (*32*). The formation of the oxidized product, tetraguaiacol, was followed at 470 nm using an extinction coefficient ϵ_{470} of 26 600 M^{-1} cm^{-1}. Ferrocyanide peroxidase activity was determined in 17 mM $K_4Fe(CN)_6 \cdot 3H_2O$, 600 μM H_2O_2, and 10 nM WTCcP or N195PK2 in 5 mM or 100 mM Tris-phosphate, pH 6.0 (*16*). The formation of oxidized product, ferricyanide, was monitored at 420 nm using an extinction coefficient ϵ_{420} of 1000 M^{-1} cm^{-1}.

The following conditions were employed to measure steady-state activity as a function of cation concentration. N195PK2 was added to 5 or 100 mM Tris-phosphate, pH 6.0 (Na^+/K^+ free), containing K^+ or other ions at various concentrations, and then 180 μM H_2O_2 and 30 μM horse heart or yeast cyt *c* were added in concert to begin the reaction. Tris-base (Na^+/K^+ free) (1 M) was equilibrated to pH 6.0 with ion-free phosphoric acid purchased from Aldrich Chemicals. Results are presented as turnover numbers (k_{cat}) as a function of [K^+]. Dissociation constants (K_d) were estimated by fitting the data to titration curves assuming a simple equilibrium between cation free and bound enzyme and a single cation binding site.

Electron Paramagnetic Resonance (EPR) Spectroscopy. EPR spectra were recorded on a Bruker ESP300 spectrophotometer equipped with an Air Products LTR3 liquid helium cryostat. Experimental conditions used to record Trp191 cation radical formation of the wild-type protein and mutants were as follows: microwave frequency, 9.475 GHz; microwave power, 0.5 mW; modulation amplitude, 4.57 G; modulation frequency, 100 kHz; field sweep rate, 11.92 G/s; time constant, 0.0256 ms; and receiver gain, 1.0×10^4 (wild-type) and 2.5×10^4 (N195PK2). The resting state sample had WTCcP and N195PK2 at 300 μM in 5 mM Tris-phosphate, pH 6.0, with or without cations in a total volume of 150 μL. Compound I was formed by the addition of an equal volume of 360 μM H_2O_2 in respective buffers, and the samples were frozen in quartz EPR tubes by submersion in a mixture of *n*-hexanes chilled into a slurry with liquid nitrogen, immediately or at defined time intervals. Spectra were recorded at 8 K. The data obtained were an average of 10 scans.

Spectral Titrations with 1,2-Dimethylimidazolium (DMI). Binding assays were performed by difference absorption spectroscopy using a Cary 3E UV−visible spectrophotometer at 20 °C (*18*). Stock solutions of DMI were prepared with 100 mM bis-tris-propane/MES, pH 6.0. Stock protein solutions of CcP were also prepared in 100 mM bis-tris-propane/MES, pH 6.0, so as to give an absorbance of 1.0 at the Soret maximum (10.34 μM). Protein solutions were allowed to equilibrate at 20 °C for 30 min in the spectrophotometer and the instrument blanked. An aliquot of DMI stock solution (10 μL of 1 M DMI for mutant CcP and 5 M DMI for WTCcP) was added to the cuvette, allowed to equilibrate, and the difference spectrum recorded. Difference spectra were recorded until saturation was reached. Dissociation constants (K_d) were determined from the changes in the Soret maximum of the heme using the same curve fitting procedures employed for the cation titration experiments.

Crystallization, X-ray Data Collection and Structure Refinement. Diffraction quality crystals were prepared in 30% 2-methyl-2,4-pentanediol (MPD), 50 mM KPB, pH 6.0, according to Edwards and Poulos (33) as later modified by Sundaramoorthy et al. (*34*). A lower initial concentration of N195PK2, 200 μM (∼6.4 mg/mL), than previously reported was used to grow smaller 0.2 mm crystals from touch seeding. This smaller size crystal was necessary for better cryogenic freezing and to avoid twinning during crystal growth. X-ray intensity data were collected from a single flash frozen crystal using an R-AXIS IV imaging plate on a Rigaku rotating anode X-ray source equipped with a Crystal Logic cryogenic N_2 delivery system. Initial image processing, indexing, and integration were performed with *DENZO* version 1.9.1, and the integrated data were scaled using

Table 1: Statistics of Data Collection and Refinement of N195PK2 and CcPK2

	N195PK2	CcPK2
data collection		
space group	$P2_12_12_1$	$P2_12_12_1$
unit cell dimension		
a (Å)	106.68	106.41
b (Å)	75.34	75.39
c (Å)	51.30	51.18
total reflections	315 272	262 488
unique reflections	33 299	33 436
resolution (Å)	1.9	1.9
I/σ last shell	4.19	8.87
completeness full dataset (%)	99.4	98.1
completeness last shell (%)	99.5	96.1
R-factor (R_{symm})[a]	0.088	0.051
refinement		
resolution range (Å)	50.0−1.9	50.0−1.9
no. of reflections	32 159	32 224
R_{cryst}[b]	0.1582	0.1622
R_{free} (5% data set aside)	0.199	0.1932
rms bond lengths (Å)[c]	0.0052	0.0051
rms bond angles (deg)[c]	2.2523	2.6931
no. of solvent molecules	730	606

[a] $R_{sym} = \sum|I_{obs} - I_{avg}|\bar{\sum}I_{avg}$. [b] $R_{cryst} = \sum(|F_{obs}| - |F_{calc}|)/\sum|F_{obs}|$. [c] rms bond and rms angle represent the root-mean-squared deviation between the observed and ideal values.

SCALEPACK version 1.9.0 (*34*). Summary of data collection is provided in Table 1.

The starting model for refinement was CcPCa2 obtained at cryogenic temperatures. Tom (version 3.0) was used to replace D192T, T194N, and N195P. The model was fitted to N195PK2 data using rigid body refinement as implemented in *CNS* (version 1.0) (*36*). Next, 5% of the data were set aside to calculate R_{free} for cross-validation (*37*). To begin refinement of the model, simulated annealing starting at 3000 K as implemented in *CNS* was used to remove any previous model bias. The subsequent refinements involved multiple rounds of model building in Tom (version 3.0), with positional refinement for 100 cycles followed by *B*-factor refinement for 30 cycles with *CNS*. Alternative conformations were modeled for residue positions Arg48 and Arg166 and water molecules 65 and 474. In addition 730 ordered solvent molecules were added to the molecular model. To compare these data with CcPK2 structure, the CCPK2 data obtained at Stanford Synchotron Radiation Laboratory (SSRL) beamline 7-1 was indexed, scaled, and refined to the same resolution as N195PK2 using *CNS*. The final refinement parameters of CcPK2 and N195PK2 are summarized in Table 1.

RESULTS

Crystal Structures. Figure 1 shows the location of the K^+ site in the engineered CcP while Figure 2 provides a sequence alignment of the proximal cation-binding loop in various peroxidases. Although the backbone polypeptide conformation of CcP and other peroxidases are nearly identical in the proximal cation-binding loop region, CcP lacks the side chain ligands that would bind the metal ion and hence binds water rather than a cation at this position. We had previously engineered CcP to mimic APX in binding K^+ by changing five crucial residues, viz. A176T, G192T, A194N, T199D, and E201S (*10*, *24*). This mutant was called CcPK2. The

WTCcP	**A**^{176}	.....	**G**^{192}	A	**A**	N	N	**V**	F	**T**	N	E^{201}
APX	**T**^{164}	.....	**T**^{180}	S	**N**	P	L	**I**	F	**D**	N	S^{189}
LIP	**S**^{177}	.....	**D**^{194}	S	**T**	P	G	**I**	F	**D**	S	Q^{203}
CcPK2	**T**^{176}	.....	**T**^{192}	A	**N**	N	N	**V**	F	**D**	N	S^{201}
CcPCA1	**T**^{176}	.....	**D**^{192}	A	**N**	N	N	**V**	F	**D**	N	S^{201}
CcPCA2	**T**^{176}	.....	**D**^{192}	A	**T**	N	N	**V**	F	**D**	N	S^{201}
N195PK2	**T**^{176}	.....	**T**^{192}	A	**N**	P	N	**V**	F	**D**	N	S^{201}

FIGURE 2: Sequence alignments of the cation-binding loop in various peroxidases. Side chain ligands are in bold face. The remaining ligands are provided by peptide carbonyl oxygen atoms. *WT*, wild-type; *APX*, ascorbate peroxidase; *LIP*, lignin peroxidase; *CcPK2*, *CcPCa1*, *CcPCa2*, and *N195PK2*, mutants of WTCcP.

current mutant, N195PK2 was generated on CcPK2. The higher resolution structure of CcPK2, refined in *XPLOR* at 1.5 Å from data obtained at SSRL, provided a more accurate description of the engineered cation site. To see if the N195P mutation had brought about any changes in the cation-binding loop, the crystal structure of N195PK2 was determined and refined to 1.9 Å resolution using *CNS*. To obtain an accurate and reliable comparison, the CcPK2 structure obtained at SSRL was also refined to the same resolution in *CNS*. During the course of refinement, no constraints or restraints were used between the ligand and cation in order to provide an unbiased set of ligand−cation distance parameters. A $2F_o - F_c$ omit electron density map of N195PK2 is shown in Figure 3. The map shows all side chain ligands of potassium to be intact with no perceptible change in the cation-binding environment except for the presence of Pro195. When modeled as K^+ with full occupancy, the temperature factor (*B*-factor) refined to 11.39 Å^2, which compared favorably with 10.4 to 11.74 Å^2 range for the seven oxygen ligand atoms to the cation in a distorted pentagonal bipyrimidal geometry. In addition, the *B*-factors of the cation-binding loop of CcPK2 and N195PK2 agreed nicely indicating that the N195P mutation had neither altered the cation-binding properties of the mutant nor the cation-binding oxygen ligands.

As a basis for comparison, the structure of cation-binding site of N195PK2 in relation to CcPK2 and APX is provided in Figure 4. In addition to the better CcPK2 structure, the APX structure had been refined to a higher resolution using a 1.8 Å cryogenic dataset (*38*). This enables a more accurate and direct comparison of bond distances and angles among the CcPK2, N195PK2 and APX cation-binding loops, as shown in Table 2. The N195P mutation did not alter the hydrogen bond between the side chain amide nitrogen on Asn194 and the side-chain carboxylate oxygen of Asp199 (Figure 4). This critical hydrogen bond also seen in APX and CcPK2 is critical for the stability of cation-binding loop. Even more importantly, this hydrogen bond helps to orient the other carboxylate oxygen of Asn194 side chain to point inward becoming a ligand to the cation.

The current model of N195PK2, similar to CcPK2, also showed several alternative side chain conformations. Of particular relevance is Arg48, a residue in the distal pocket involved in the formation and stabilization of compound I, which is in two positions as in CcPK2, which we have termed "*in*" and "*out*". The *out* conformation is the same as the room temperature 1.7 Å structure of WTCcP (*39*) while the *in* conformation is similar to what is found in compound I (*10*, *24*, *40*, *41*) and the fluoride complex (*42*). The "*in*"

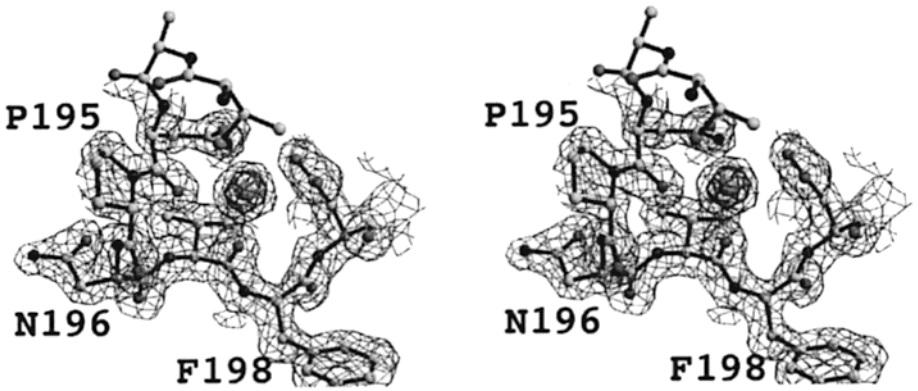

FIGURE 3: Stereoviews of the $2F_o - F_c$ omit electron density map of N195PK2. The maps were contoured at 1.0 and 5.0σ. The models were subjected to one round of simulated annealing refinement as implemented in *CNS* starting at 3000 K with the atoms shown excluded from the refinement. The K^+-binding loop is well ordered retaining all the cation-binding side chain ligands.

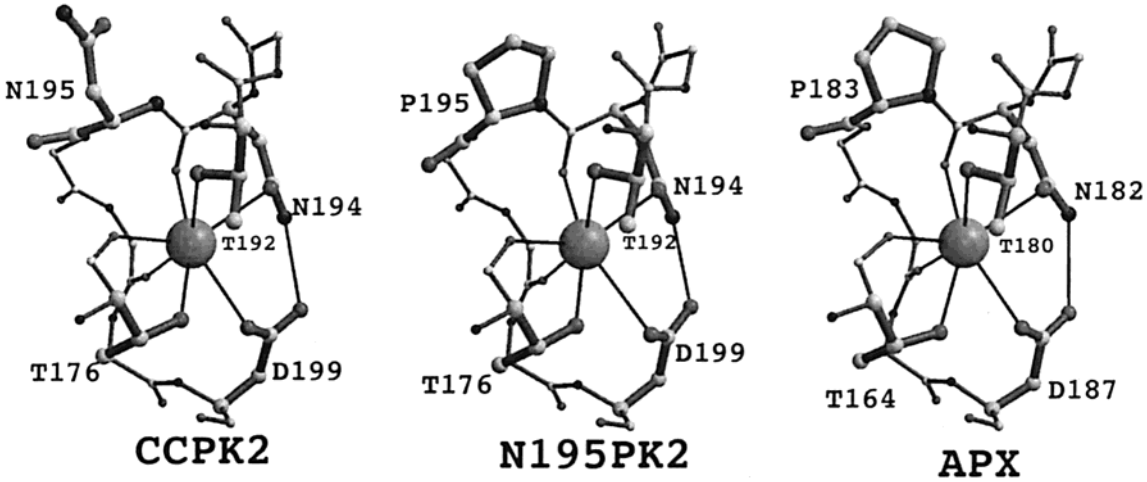

FIGURE 4: Models of the cation-binding sites in the engineered CcP mutants and ascorbate peroxidase. *CcPK2* and *N195PK2*, K^+-binding CcP mutants; *APX*, ascorbate peroxidase

Table 2: Comparison of Cation (K^+) to Ligand Distances

residue in CcP (APX) (distance in Å)	CcPK2	N195PK2	APX
Thr 176 (164) OG1	2.64	2.69	2.57
Thr 176 (164) C═O	2.69	2.60	2.88
Thr 192 (180) OG1	3.00	2.93	2.96
Asn 194 (182) C═O	2.72	2.68	2.77
Asn 194 (182) OD1	2.79	2.76	2.74
Val 197 (185) C═O	2.76	2.75	2.61
Asp 199 (187) OD1	3.05	3.31	2.99
H-bond from Asn 194 (182) ND2 to Asp 199 (187) OD2	2.92	2.83	2.86

conformation enables Arg48 to directly interact with ligands coordinated to the heme iron or, in the case of high-spin ferric complex, to an ordered water molecule situated over the iron. Similarly, Arg166 exists in alternate side chain conformations much in the same way as CcPK2.

Steady-State Kinetics. N195PK2 has only ~10% of the steady-state activity of WTCcP toward horse heart cyt *c* similar to CcPK2 in the absence of K^+. Increasing concentrations of K^+ or Na^+ brought about another 10-fold loss in activity in N195PK2. However, the concentration of Na^+ required for maximum inhibition is about 100-fold higher than required for K^+ inhibition which demonstrates specificity for K^+ (Figure 5). As discussed in earlier publications (*10*, *24*, *43*), mutations alone contributed to a substantial loss in activity and addition of increasing [K^+] using both low and high ionic strength buffers led to another 10-fold loss due to long-range electrostatic effects (Figure 5, panels A and B). Although addition of Na^+ also caused ~10-fold loss in activity (Figure 5D), it required higher concentrations than potassium, indicating ion specificity and selectivity. From the data in Figure 5 the estimated K_d values for K^+ and Na^+ are 3.3 ± 0.3 μM and 347.7 ± 4.5 μM, respectively. None of the other monovalent or divalent cations had any significant influence on activity confirming the specificity for K^+ and to a lesser extent Na^+, an ion with similar charge and size.

In previous studies we used only horse heart cyt *c* as a substrate. Here, however, we have also used yeast cyt *c*, which led to some interesting results. In low ionic strength buffer, N195PK2 exhibited a similar activity to that of WTCcP (Figure 6A) and increasing K^+ had only a moderate effect on both WTCcP and N195PK2. In high ionic strength buffer without added K^+, N195PK2 exhibited 37-fold lower activity relative to WTCcP (Figure 6B), and increasing K^+ led to another 3-fold loss in activity (Figure 6B, inset), while WTCcP was largely unaffected. Eadie-Hofstee plots for N195PK2 gave similar kinetic constants for substrate binding as WTCcP (data not shown) indicating that the affinity for both horse heart and yeast cyt *c* is not altered.

The steady-state activity was also determined using two small molecule substrates, guaiacol, and potassium ferrocyanide under conditions of saturating substrate. N195PK2

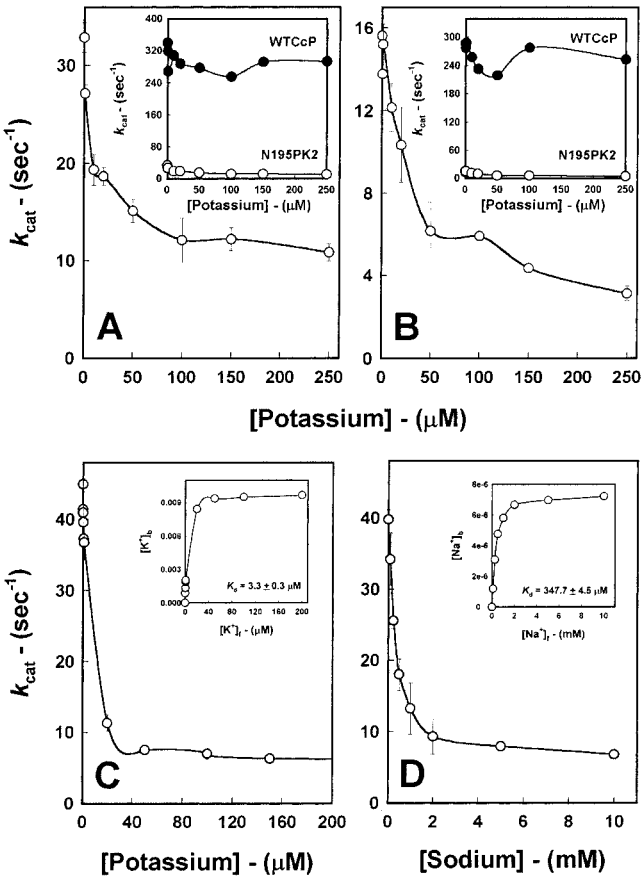

FIGURE 5: Kinetic titration data of N195PK2 with reduced horse heart cytochrome *c*. Titration of steady-state activity wild-type CcP (closed circles) and N195PK2 (open circles) with $[K^+]$. A steady-state assay was carried out on N195PK2 at various concentrations of K^+. Assays were carried out in 5 mM or 100 mM Tris-phosphate, pH 6.0 containing 250 pM (WTCcP) or 10 nM (N195PK2) enzyme, 180 μM hydrogen peroxide and 30 μM ferrocytochrome *c* at the indicated concentration of ions. The experimental details are provided under Materials and Methods. (A) In 5 mM Tris-phosphate, pH 6.0, and (B) in 100 mM Tris-phosphate, pH 6.0. Panels C and D show the titration curves for K^+ (panel C) and Na^+ (panel D). The insets in panels C and D are computer fits to the data assuming a simple equilibrium with one binding site. K_d values were computed from these plots.

exhibited 26.2% of the WTCcP levels using ferrocyanide as the substrate, but the activity toward guaiacol was the same as wild-type levels (data not shown). The steady state kinetic behavior of N195PK2 is similar to CcPK2 except in our earlier studies with CcPK2 we used only horse heart cyt *c* as a substrate.

Single Turnover Experiments. Since the Trp191 radical is unstable in the CcPK2 and N195K2 mutants, it was not possible to test if the short-lived Trp191 radical still can accept an electron from ferrocyt *c* using the normal technique of mixing preformed CcP compound I with ferrocyt *c* using a stopped-flow system. Alternatively, one can mix a 1:1 combination CcP-ferrocyt *c* with excess H_2O_2, which will generate compound I followed by electron transfer from ferrocyt *c*. However, under these conditions, the rate of intramolecular electron transfer was too fast to be measured by conventional stopped-flow methods. We therefore carried out the following experiment using a simple UV−visible spectrophotometer. One equivalent of ferrocyt *c* was mixed with CcP, and the spectrum recorded. One equivalent of H_2O_2

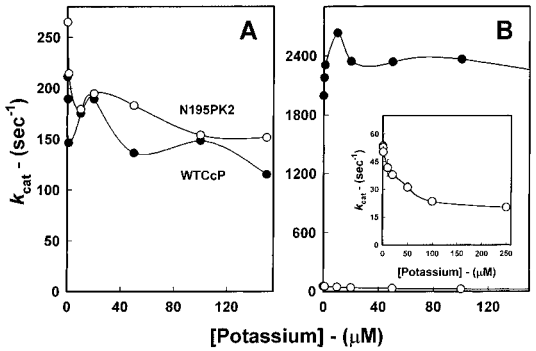

FIGURE 6: Kinetic titration data of N195PK2 with reduced yeast cytochrome *c*. Stead-state assays of wild-type CcP (closed circles) and N195PK2 (open circles) were carried out in 5 or 100 mM Tris-phosphate, pH 6.0 containing 250 pM wild-type CcP or 10 nM N195PK2, 180 μM hydrogen peroxide, and 30 μM reduced yeast cytochrome *c* at the indicated concentrations of potassium. The experimental details are provided under Materials and Methods. (A) In 5 mM Tris-phosphate, pH 6.0, and (B) In 100 mM Tris-phosphate, pH 6.0.

was added, and the spectrum recorded again. Under these conditions the ferrocyt *c* should be completely oxidized by CcP compound I. If the ferrocyt *c* transfers an electron to the Trp191 radical, then the characteristic spectral properties of compound I due to the $Fe^{4+}O$ center will be unperturbed since the Trp191 radical does not contribute significantly to the visible absorption spectrum. If these conditions are met then the spectrum of CcP-ferrocyt *c* + H_2O_2 will be the same as CcP + oxidized cyt *c* + H_2O_2. This is precisely what we observe for both WTCcP and N195PK2 using both horse heart and yeast ferrocyt *c*. This means that one full equivalent of the Trp191 radical forms in N195PK2 compound I, which can accept an electron from either horse heart or yeast ferrocyt *c* exactly as in WTCcP.

EPR Spectroscopy. If the introduced mutation resulted in 10-fold loss of enzyme activity due to instability of the Trp^+ radical then it should be reflected in the EPR signal of compound I. The EPR signal of the compound I Trp^+ radical of CcP was typically axially symmetric with a broad envelope due to Trp191 radical being exchange coupled to $S = 1$ oxyferryl heme iron center with a $g = 2.01-2.04$. Indeed, when the compound I Trp^+ radical signal of N195PK2 was monitored as a function of time of freezing, the radical signature decreased with time and vanished in about 20 min (Figure 7B). These spectral features also indicate that the nature of the coupling between the Trp191 free radical and heme has been significantly altered. In sharp contrast, the WTCcP EPR signal was stable for nearly 2 h (Figure 7A). It is clear from the Figure 8A that the EPR signal of N195PK2 gets progressively weaker as $[K^+]$ goes above 1 μM. To some extent increasing $[Na^+]$ also decreased the compound I Trp^+ radical (Figure 8B) but the concentrations required were much higher than K^+. There is a slight increase in the EPR signal up to 1 μM K^+ which suggests that at low concentrations K^+ might stabilize the radical. The close parallel in the loss of activity and diminishing EPR signal supports our earlier conclusions that activity loss is due to an electrostatic effect that destabilizes the Trp191 cation radical in the presence of bound potassium. As expected, the EPR properties of the N195K2 mutant compound I are similar to that of CcPK2 including the ion selectivity for potassium.

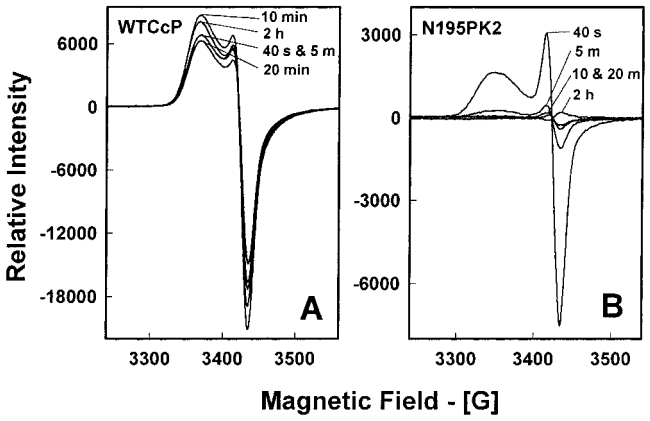

FIGURE 7: Trp191 EPR radical signal of wild-type and N195PK2 cytochrome *c* peroxidase. The EPR Trp191 radical signal of wild-type and N195PK2 compound I in the absence of cations was monitored as a function of time of freezing the compound I. Enzyme (300 μM) was mixed with 360 μM H_2O_2 in 5 mM Tris-phosphate, pH 6.0 and the compound I formed was frozen in EPR tubes at different defined time intervals as mentioned in the figure and their EPR spectra recorded. The data obtained were an average of 10 scans. The experimental conditions are described under Materials and Methods. (A) WTCcP, and (B) N195PK2.

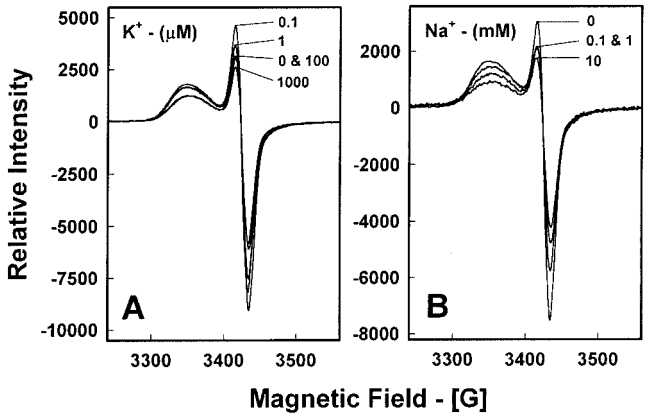

FIGURE 8: Titration of the Trp191 EPR radical signal of N195PK2 with [K^+] and [Na^+]. The EPR signal of N195PK2 compound I Trp191 radical was considerably weaker than wild-type CcP, which correlated with the loss of activity. Enzyme (300 μM) was mixed with 360 μM H_2O_2 in 5 mM Tris-phosphate, pH 6.0, in the absence and presence of differing [K^+] or [Na^+] and the compound I formed were frozen immediately and their EPR spectra recorded. The data obtained were an average of 10 scans. The experimental conditions of titration are described under Materials and Methods. (A) WTCcP, and (B) N195PK2

Spectral Titrations with 1,2-Dimethylimidazolium. The section of polypeptide containing Trp191 and the 190−195 segment of the cation-binding loop can exist in two conformations which are in equilibrium: one with the Trp191 in its native position (*closed*) and one with Trp191 extending out in solution ~10 Å from its native position (*open*) (*21*). This leaves an open pocket formerly occupied by Trp191 that is capable of binding DMI, thus leading to easily detectable spectral changes which can be used to follow the loop *open/closed* conformational equilibrium (*25*). In our earlier work with CcPK2, we found that DMI bound more tightly and faster to CcPK2 with or without K^+, indicating that the mutations had destabilized the loop to favor the *open* conformation (*24*). The apparent K_d for CcPK2 was found to be 54.47 mM compared to 172.4 mM for WTCcP. As shown in Figure 9A we found that N195PK2 bound DMI with an apparent K_d of 53.94 + 7 mM (Figure 9A, inset), similar to CcPK2 suggesting that the loop more readily adopts an *open* conformation. However, when N195PK2 was titrated with DMI in the presence of 10 μM potassium, there was little change in the difference spectrum as shown in Figure 9B which precludes an accurate estimate of K_d. From these observations we conclude that in the absence of bound K^+ in the cation-binding loop, Trp191 more readily adopts an *open* conformation, while in the presence of K^+, the *closed* conformation is favored just as in WTCcP. This effect was specific for K^+ since DMI binding to N195PK2 was unaffected by the presence of either Na^+ or Ca^{2+} as indicated by difference absorption spectroscopy and similar K_d values (data not shown). This again confirms the specificity of cation-binding loop to K^+ and shows that by installing Pro at 195 the cation-binding loop is rigidified in the presence of K^+.

DISCUSSION

Stability of the Cation Loop. Results presented in this and previous studies support the view that the engineered cation site acts as a molecular switch in modulating the stability of the Trp191 cationic radical. The presence of a cation ~8 Å away from Trp191 presumably causes electrostatic destabilization of the positive charge on the Trp191 cation radical. However, as the mutations alone destabilize the loop it was difficult to separate the effects of the mutations alone on radical stability from the effect of the bound cation (*24*). The initial goal of this study was to try and stabilize the engineered cation-binding loop in CcP such that the functional effects of K^+ binding and the mutations alone could be separately analyzed. The first step was to ensure that the conversion of Asn 195 to Pro did not alter the structure. As expected, N195PK2 still binds K^+ and there is no structural change other than the replacement of Asn with Pro.

Our earlier work (*10*, *24*, *43*) showed that mutations alone in the absence of K^+ cause destabilization of Trp191 cationic radical, resulting in a corresponding loss in enzyme activity. One of the plausible explanations emerged from the work of Cao et al. (*21*) who showed, based on crystal structures, that CcP exists in a mixture of *open* and *closed* conformations and the two conformers are in equilibrium. The *closed* form has Trp191 in its native position observed in the crystal structures while in the *open* form, Trp191 moves ~10 Å to the molecular surface, owing to a large movement of the surface loop consisting of residues 190−195. The cavity created in the proximal cation-binding loop enables it to bind protonated forms of small cationic imidazole derivatives such as 1,2-dimethylimidazolium (DMI). This binding of DMI to Trp191 site results in an easily detectable spectral shift to a low-spin signal, which provides a simple method for following the *open*/*closed* equilibrium.

$$\text{closed} \leftrightarrow \text{open} \xleftrightarrow{\text{DMI}} \text{open}-\text{DMI}$$

At any given time, some fraction of the protein is in the *open* conformation, which represents a small percentage of the population. DMI selects this conformer and shifts the loop *closed/open* equilibrium toward the *open* conformer (*18*).

The structural changes in going from *closed* to *open* conformations involve two key hinge residues, Pro190 and

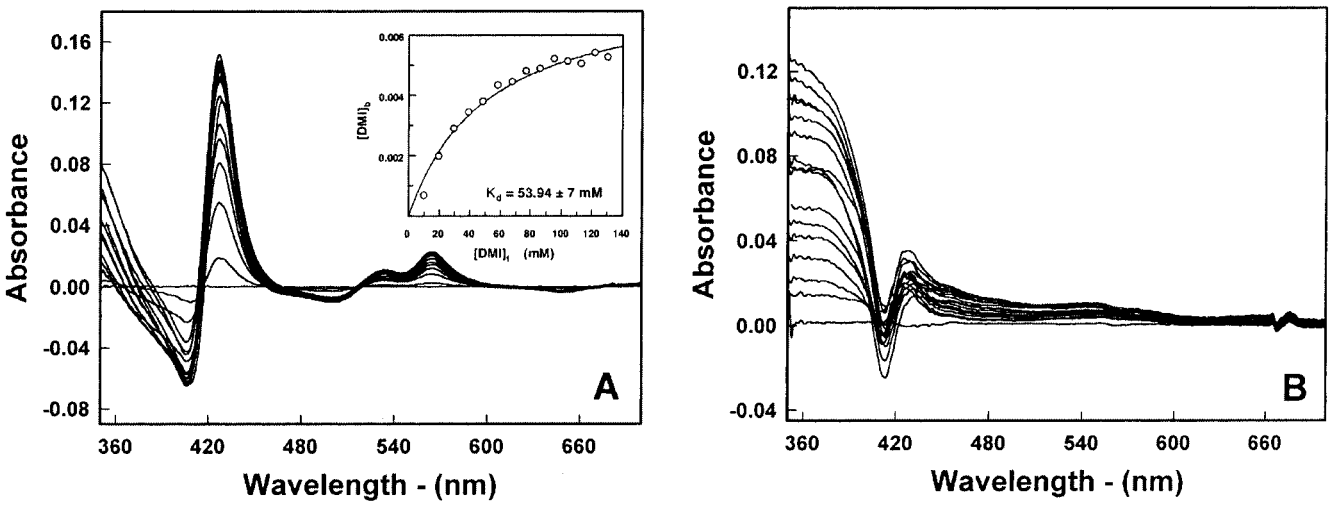

FIGURE 9: Binding of DMI to N195PK2. Optical difference spectra of a typical spectral titration curve for N195PK2 with DMI is shown both in the absence of K^+ (A) and in the presence of stoichiometric concentrations of K^+ (10 μM) (B) The fraction of DMI bound, $[DMI]_b$, was determined by extrapolating $1/\Delta A_{412}$ vs $1/[DMI]_t$ to infinite [DMI] assuming one binding site. The detailed experimental conditions are provided under Materials and Methods. The inset in panel A is a computer fit to the data assuming a simple equilibrium with one binding site. K_d was computed from this plot.

Asn195 (*25*). Pro190 undergoes a *trans* to *cis* isomerization, and Asn195 side chain switches positions with main chain atoms (*21*, *25*). Our initial engineering efforts were directed toward changing the cation ligand residues to corresponding residues in APX. The next step was to introduce the entire cation-binding loop of APX. APX has Pro183, which is Asn195 in CcPK2 and WTCcP, at the hinge region. Since Asn195 is a key residue in the *closed* to *open* conformational switch, we reasoned that, by changing Asn195 to Pro, the cation-binding loop may well be rigidified which would prevent the switch to *open* conformation. The present work shows that, as predicted, changing Asn195 to Pro stabilizes the loop, but only in the presence of K^+. Therefore, the effect of K^+ on the mutant EPR and activity properties can be attributed to K^+ binding and not loop instability.

We recently attempted the *inverse* experiment by removing the K^+ site in ascrobate peroxidase (APX) in an attempt to "turn on" the Trp radical in this peroxidase (*44*). However, the K^+-free APX mutant underwent a large conformational change generating a species that has two His ligands to the Fe^{3+} center, most likely due to the distal His coordinating the heme iron. Given that the engineered cation site in CcP is nearly identical to APX, it is not surprising that the mutant CcP cation loop now requires a bound cation for stability.

Stability of the Trp191 Radical. Our single turnover experiments show that the engineered K^+ site does not alter the formation of the Trp191 radical but only its stability. When 1 equiv of H_2O_2 is added to a 1:1 mix of N195PK2 plus horse heart or yeast ferrocyt *c*, the ferrocyt *c* is completely oxidized and the CcP compound I spectrum due to the Fe^{4+}-O heme is unaltered, indicating that the Trp191 radical must have received the electron from ferrocyt *c*. Hence, the engineered cation site does not prevent Trp191 from being fully oxidized and serving as the electron entry site from ferrocyt *c*. As indicated by the EPR results, the main effect of the engineered cation site is on the stability of the Trp191 cation radical and not its initial formation. The EPR spectral features of the mutant are quite different than in WTCcP possibly suggesting another neighboring site has been oxidized. However, the single turnover results indicate that Trp191 was fully oxidized. Moreover, the Trp191 EPR signal is known to be extremely sensitive to the effects of mutations by altering the exchange coupling between the Trp191 radical and heme iron (*5*, *28*, *45*).

It seems likely that the bound cation increases the redox potential of Trp191, but not to the extent that the heme or some other neighboring side chain (probably Tyr) is preferentially oxidized. As indicated by recent theoretical studies (*19*), the cation contributes part, but not all, of the difference between APX and CcP in the ability to stabilize the Trp cation radical. In theory, it should be possible to continue to engineer CcP such that the redox potential of Trp191 will be sufficiently high that some other group, most likely the heme porphyrin macrocycle, will be preferentially oxidized. At least this is the prediction if the local electrostatic environment is the primary determinant of redox potentials and cation radical stability.

Steady-State Activity. It is generally thought that small phenolic substrates such as guaiacol deliver an electron to the exposed *δ-meso* heme edge (*46*) while a larger charged substrate like ferrocyanide must bind on the surface of CcP, possibly at or near the same site utilized by cyt *c*. Hence, guaiacol delivers its electron directly to the heme edge while ferrocyanide utilizes the same electron-transfer path as cyt *c*, namely, through the Trp191 cationic radical. Introduction of the K^+ binding loop into CcP should effect only the path of electron transfer that requires formation of a stable Trp191 radical. This is the most likely reason N195PK2 has a reduced activity toward ferrocyanide but not guaiacol.

Our previous work utilized horse heart ferrocyt *c* as the substrate and under all conditions tested, the K^+-binding CcP mutants are much less active than WTCcP. In the present study we also used yeast ferrocyt *c* and in this case the N195PK2 is as active as WTCcP at low ionic strength with no K^+-dependence on activity. However, at higher ionic strength, the mutant activity can be titrated away with K^+. To interpret this difference first requires a better understand-

ing of how the reduction of compound I is thought to proceed. The following outlines the currently favored view:

$$Fe^{4+}Trp^{\bullet+} + \text{cyt } c\ (Fe^{2+}) \rightarrow Fe^{4+}Trp^{\bullet+}/\text{cyt } c\ (Fe^{2+}) \quad (1)$$

$$Fe^{4+}Trp^{\bullet+}/\text{cyt } c\ (Fe^{2+}) \rightarrow Fe^{4+}Trp/\text{cyt } c\ (Fe^{3+}) \quad (2)$$

$$Fe^{4+}Trp/\text{cyt } c\ (Fe^{3+}) \rightarrow Fe^{4+}Trp + \text{cyt } c\ (Fe^{3+}) \quad (3)$$

$$Fe^{4+}Trp \leftrightarrow Fe^{3+}Trp^{\bullet+} \quad (4)$$

In *step 1*, CcP forms a complex with ferrocyt *c* followed by electron transfer (*step 2*) and dissociation (*step 3*) of oxidized cyt *c*. *Step 4* represents the intramolecular electron transfer from Trp191 to the iron giving Fe^{3+} $Trp^{\bullet+}$ the intermediate required to oxidize the second molecule of ferrocyt *c*. In this mechanism formation of the Trp191 cation radical is essential for both electron-transfer steps.

It is well-known that horse heart and yeast cyt *c* behave very differently under both steady-state conditions and in single turnover experiments. An extensive analysis of the steady-state CcP reaction using yeast ferrocyt *c* as the substrate led to the conclusion that the rate-limiting step under steady-state conditions is dissociation of the cyt *c*−CcP complex (*8*) at ionic strengths below 150 mM (*47*). At high ionic strength the rate-limiting step switches to intramolecular electron transfer from Trp191 to Fe^{3+} (*step 4*) (*47*). An additional complication is that a second low-affinity site for yeast ferrocyt *c* on CcP (*48*−*51*), which is not active in electron transfer (*52*), promotes dissociation of cyt *c* from the active high-affinity site (*8*, *47*). In sharp contrast, horse heart ferrocyt *c* has only one binding site on CcP (*53*) and is a poorer substrate under steady-state conditions at high ionic strength (*54*, *55*). It also is well-known that when yeast ferrocyt *c* is the substrate, CcP activity can vary by as much as 10−20-fold as a function of ionic strength (*56*), similar to what we find in the present study.

We suggest that the key to understanding why N195PK2 retains wild-type levels of activity using yeast ferrocyt *c* as the substrate is because the rate-limiting step changes as a function of ionic strength for yeast, but not for horse heart ferrocyt *c*. Since product dissociation is limiting for yeast cyt *c* at low ionic strength, the intramolecular electron-transfer rate of $\sim$50 000 s^{-1} (*14*) from yeast ferrocyt *c* to the Trp^+ radical is sufficiently fast to reduce even the short-lived Trp^+ radical in the mutant. However, at higher ionic strength the rate-limiting step switches to intramolecular electron transfer in CcP from Trp191 to Fe^{4+} (*47*). Once intermolecular electron-transfer becomes part of the rate-limiting step, then the stability of the Trp^+ radical becomes more important. This is why at higher ionic strength K^+ begins to decrease the activity of N195PK2 when yeast ferrocyt *c* is the substrate (Figure 6). The addition of K^+ decreases the stability of the Trp191 radical which affects the Trp191 to Fe^{4+} intramolecular electron-transfer reaction and hence, lowers the observed steady-state activity (Figure 6). We suggest that, with horse heart cyt *c*, the rate-limiting step does not change as a function of ionic strength, but remains at the Trp191 to Fe^{4+} intramolecular electron-transfer reaction.

ACKNOWLEDGMENT

We thank William Lanzalotta for his technical expertise in EPR spectroscopic experiments.

REFERENCES

1. Poulos, T. L., Freer, S. T., Alden, R. A., Edwards, S. L., Skogland, U., Takio, K., Eriksson, B., Xuong, N., Yonetani, T., and Kraut, J. (1980) *J. Biol. Chem. 255*, 575−580.
2. Finzel, B. C., Poulos, T. L., and Kraut, J. (1984) *J. Biol. Chem. 259*, 13027−13036.
3. Erman, J. E., Vitello, L. B., Mauro, J. M., and Kraut, J. (1989) *Biochemistry 28*, 7992−7995.
4. Sivaraja, M., Goodin, D. B., Smith, M., and Hoffman, B. M. (1989) *Science 245*, 738−740.
5. Houseman, A. L., Doan, P. E., Goodin, D. B., and Hoffman, B. M. (1993) *Biochemistry 32*, 4430−4443.
6. Huyett, J. E., Doan, P. E., Gurbriel, R., Houseman, A. L. P., Sivaraja, M., Goodin, D. B., and Hoffman, B. M. (1995) *J. Am. Chem. Soc. 117*, 9033−9041.
7. Erman, J. E., and Yonetani, T. (1975) *Biochim. Biophys. Acta 393*, 343−349.
8. Miller, M. A. (1996) *Biochemistry 35*, 15791−15799.
9. Pelletier, H., and Kraut, J. (1992) *Science 258*, 1748−1755.
10. Bonagura, C. A., Sundaramoorthy, M., Pappa, H. S., Patterson, W. R., and Poulos, T. L. (1996) *Biochemistry 35*, 6107−6115.
11. Hahm, S., Green, L., Durham, B., and Millett, F. (1993) *J. Am. Chem. Soc. 115*, 3372−3373.
12. Hahm, S., Miller, M. A., Geren, L., Kraut, J., Durham, B., and Millett, F. (1994) *Biochemistry 33*, 1463−1480.
13. Pappa, H. S., Tajbaksh, S., Saunders, A. J., Pielak, G. J., and Poulos, T. L. (1996) *Biochemistry 35*, 4837−4845.
14. Geren, L., Hahm, S., Durham, B., and Millett, F. (1991) *Biochemistry 30*, 9450−9457.
15. Miller, M. A., Liu, R. Q., Hahm, S., Geren, L., Hibdon, S., Kraut, J., Durham, B., and Millett, F. (1994) *Biochemistry 33*, 8686−8693.
16. Mauro, J. M., Fishel, L. A., Hazzard, J. T., Meyer, T. E., Tollin., G., Cusanovich, M. A., and Kraut, J. (1987) *Biochemistry 27*, 6243−6256.
17. Miller, M. A., Han, G. W., and Kraut, J. (1994) *Proc. Natl. Acad. Sci. U.S.A. 91*, 11118−11122.
18. Fitzgerald, M. M., Churchill, M. J., McRee, D. E., and Goodin, D. B. (1994) *Biochemistry 33*, 3807−3818.
19. Jensen, G. M., Bunte, S. W., Warshel, A., and Goodin, D. B. (1998) *J. Phys. Chem. B 102*, 8221−8228.
20. Menyhard, D. K., and Naray-Szabo, G. (1999) *J. Phys. Chem. B 103*, 227−233.
21. Cao, Y., Musah, R. A., Wilcox, S. K., Goodin, D. B., and McRee, D. E. (1998) *Protein Sci. 7*, 72−78.
22. Patterson, W. R., Poulos, T. L., and Goodin, D. B. (1995) *Biochemistry 34*, 4342−4345.
23. Patterson, W. R., and Poulos, T. L. (1995) *Biochemistry 34*, 4331−4341.
24. Bonagura, C. A., Sundaramoorthy, M., Bhaskar, B., and Poulos, T. L. (1999) *Biochemistry 38*, 5538−5545.
25. Fitzgerald, M. M., Musah, R. A., McRee, D. E., and Goodin, D. B. (1996) *Nat. Struct. Biol. 3*, 626−631.
26. Kunkel, T. A., Roberts, J. D., and Zokour, R. A. (1987) *Methods Enzymol. 154*, 367−382.
27. Darwish, K., Li, H. Y., and Poulos, T. L. (1991) *Protein Eng. 4*, 701−708.
28. Choudhury, K., Sundaramoorthy, M., Hickman, A., Yonetani, T., Woehl, E., Dunn, M. F., and Poulos, T. L. (1994) *J. Biol. Chem. 269*, 20239−20249.
29. Fishel, L. A., Villafranca, J. E., Mauro, J. M., and Kraut, J. (1987) *Biochemistry 27*, 351−360.
30. Yonetani, T., Schleyer, H., and Eherenberg, A. (1966) *J. Biol. Chem. 241*, 3240−3243.
31. Fowler, R. M., and Bright, H. A. (1935) *J. Res. Natl. Bur. Stand. 15*, 493−575.

32. Miller, V. P., DePillis, G. D., Ferrer, J. C., Mauk, A. G., and Ortiz de Montellano, P. R. (1994) *J. Biol. Chem. 267*, 8936−8942.
33. Edwards, S. L., and Poulos, T. L. (1990) *J. Biol. Chem. 265*, 2588−2595.
34. Sundaramoorthy, M., Choudhury, K., Edwards, S. L., and Poulos, T. L. (1991) *J. Am. Chem. Soc. 113*, 7755−7757.
35. Otwinowski, Z., and Minor, W. (1996) *Methods Enzymol. 276*, 307−326.
36. Brunger, A. T., Adams, P. D., Clore, G. M., DeLano, W. L., Gros, P., Grosse-Kunstleve, R. W., Jiang, J. S., Kuszewski, J., Nilges, M., Pannu, N. S., Read, R. J., Rice, L. M., Simonson, T., and Warren, G. L. (1998) *Acta Crystallogr., Sect. D 54*, 905−921.
37. Brunger, A. T. (1992) *Nature 355*, 472−475.
38. Mandelman, D., Sshwarz, F. P., Li, H. Y., and Poulos, T. L. (1998) *Protein Sci. 7*, 2089−2098.
39. Finzel, B. C., Poulos, T. L., and Kraut, J. (1984) *J. Biol. Chem. 259*, 13027−13036.
40. Edwards, S. L., Nguyen, H. X., Hamlin, R. C., and Kraut, J. (1987) *Biochemistry 26*, 1503−1511.
41. Fulop, V., Phizackerley, R. P., Soltis, S. M., Clifton, I. J., Wakatsuki, S., Erman, J., Hajdu, J., and Edwards, S. L. (1994) *Structure 2*, 201−208.
42. Edwards, S. L., Poulos, T. L., and Kraut, J. (1984) *J. Biol. Chem. 259*, 12984−12988.
43. Bonagura, C. A., Bhaskar, B., Sundaramoorthy, M., and Poulos, T. L. (1999) *J. Biol. Chem. 274*, 37827−37833.
44. Cheek, J., Mandelman, D., Poulos, T. L., and Dawson, J. H. (1999) *J. Biol. Inorg. Chem. 4*, 64−72.
45. Goodin, D. B., and McRee, D. E. (1993) *Biochemistry 32*, 3313−3324.
46. DePillis, G. D., Sishta, B. P., Mauk, A. G., and Ortiz de Montellano, P. R. (1991) *J. Biol. Chem. 266*, 19334−19341.
47. Mei, H., Wang, K., McKee, S., Wang, X., Waldner, J. L., Pielak, G. J., Durham, B., and Millett, F. (1996) *Biochemistry 35*, 15800−15806.
48. Zhou, J. S., and Hoffman, B. M. (1994) *Science 265*, 1693−1696.
49. Mauk, M. R., Ferrer, J. C., and Mauk, A. G. (1994) *Biochemistry 33*, 12609−12614.
50. Zhou, J. S., Nocek, J. M., DeVan, M. L., and Hoffman, B. M. (1995) *Science 269*, 204−207.
51. Kornblatt, J. A., and English, A. M. (1986) *Eur. J. Biochem. 155*, 505−511.
52. Miller, M. A., Geren, L., Han, G. W., Saunders, A., Beasley, J., Pielak, G. J., Durham, B., Millett, F., and Kraut, J. (1996) *Biochemistry 35*, 667−673.
53. Vitello, L. B., and Erman, J. E. (1987) *Arch. Biochem. Biophys.* , 621−629.
54. Matthis, A., Vitello, L. B., and Erman, J. E. (1995) *Biochemistry 34*, 9991−9999.
55. Kim, K. L., Kang, D. S., Vitello, L. B., and Erman, J. E. (1990) *Biochemistry 29*, 9150−9159.
56. Kang, C. H., Ferguson-Miller, S., and Margoliash, E. (1977). *J. Biol. Chem. 252*, 919−926.

BI011599Y